VŠB – Technical University of Ostrava

Fázová stabilita aktinoidových karbidů
Phase stability of actinide carbides

Author: Jakub Oprštěný
Supervisor: Dominik Legut

2020

VŠB - Technical University of Ostrava
University Study Programmes
CNT - Nanotechnology Centre

Bachelor Thesis Assignment

Student:	**Jakub Oprštěný**
Study Programme:	B3942 Nanotechnology
Study Branch:	3942R001 Nanotechnology
Title:	Phase stability of actinide carbides Fázová stabilita aktinoidiových karbidů
The thesis language:	English

Description:

The actinide carbides can be used as advanced nuclear fuels for the so-called generation IV reactors (including the gas-cooled and sodium-cooled fast reactors). These carbides are promising because of their higher thermal conductivity and operational temperature (leading to more efficient heat transfer) over conventional oxide fuels (e.g. UO2). The actinides fill 5f electrons, which are crucial for electronic structure and lattice dynamics. The primary goal is to investigate phase stability of the sesquicarbides of uranium and thorium, the effect of spin-orbit interactions, the influence of the localization of the 5f electrons on the electronic structures of these actinide carbides within density functional theory. Various electronic structure models would be performed in order to determine the correct magnetic ordering and, subsequently, mechanical and thermodynamical properties.

References:

KITTEL, Ch. Introduction to solid state physics, John Wiley & Sons, 2004, ISBN: 047141526X.

MANES, L. Actinides - Chemistry and Physical Properties. Berlin, Heidelberg: Springer-Verlag, 1985. ISBN 9783540390428.

MARTIN, R. M., Electronic Structure: Basic Theory and Practical Methods, Cambridge University Press, 2004, ISBN-13: 978-0521782852.

ASCROFT N. W. and N. D. Mermin, Solid State Physics, Cengage Learning, 1976, ISBN-13: 978-0030839931.

KAXIRAS, E. Atomic and electronic structure of solids. New York: Cambridge University Press, 2003. ISBN 978-0521523394.

CHAIKIN, P. M. and T. C. LUBENSKY. Principles of condensed matter physics. Cambridge [u.a.]: Cambridge Univ. Press, 2007. ISBN 9780521794503.

SINGLETON, J., Band Theory and Electronic Properties of Solids, Oxford Master Series in Physics, 2001, ISBN-10: 0198505914.

BLUNDELL, S. Magnetism in condensed matter. Oxford: Oxford University Press, 2001. Oxford master series in condensed matter physics. ISBN 9780198505914.

GRIMVALL, G. Thermophysical properties of materials. Enl. and rev. ed. New York:Elsevier, 1999. ISBN 0444827943.

Extent and terms of a thesis are specified in directions for its elaboration that are opened to the public on the web sites of the faculty.

Supervisor: **Ing. Dominik Legut, Ph.D.**

Date of issue: 02.12.2019

Date of submission: 08.05.2020

prof. Ing. Jaromír Pištora, CSc.
Head of Department

Ing. Zdeňka Chmelíková, Ph.D.
Vice-rectress for Study Affairs

Zásady pro vypracování bakalářské práce

I.

Bakalářskou prací (dále jen BP) se ověřují vědomosti a dovednosti, které student získal během studia, a jeho schopnosti využívat je při řešení teoretických i praktických problémů.

II.

Uspořádání bakalářské práce:

1. Titulní list
2. Originál zadání BP
3. Zásady pro vypracování BP
4. Prohlášení + místopřísežné prohlášení
5. Prohlášení zástupce spolupracující právnické nebo fyzické osoby
6. Abstrakt + klíčová slova česky a anglicky
7. Obsah BP
8. Textová část BP
9. Seznam použité literatury
10. Přílohy

ad 1) Titulní list je koncipován podle požadavků příslušné oborové katedry.

ad 2) Originál zadání BP obdrží student na oborové katedře.

ad 3) Tyto „Zásady pro vypracování bakalářské práce“ následují za originálem zadání BP.

ad 4) Prohlášení + místopřísežné prohlášení napsané na zvláštním listu a vlastnoručně podepsané studentem s uvedením data odevzdání BP.

ad 5) V případě, že BP vychází ze spolupráce s jinými právnickými a fyzickými osobami a obsahuje citlivé údaje, je na zvláštním listě vloženo prohlášení spolupracující právnické nebo fyzické osoby o souhlasu se zveřejněním BP.

ad 6) Abstrakt a klíčová slova jsou uvedena na zvláštním listu česky a anglicky v rozsahu max. 1 strany pro obě jazykové verze.

ad 7) Obsah BP se uvádí na zvláštním listu. Zahrnuje názvy všech číslovaných kapitol, podkapitol a statí textové části BP, odkaz na seznam příloh a seznam použité literatury s uvedením příslušné stránky. Předpokládá se desetinné číslování.

ad 8) Textová část BP obvykle zahrnuje:

- Úvod, obsahující charakteristiku řešeného problému a cíle jeho řešení v souladu se zadáním BP;
- Vlastní rozpracování BP (včetně obrázků, tabulek, výpočtů) s dílčími závěry vhodně členěné do kapitol a podkapitol podle povahy problému;
- Závěr, obsahující celkové hodnocení výsledků BP z hlediska stanoveného zadání.

BP bude zpracována v rozsahu min. 35 stran (včetně obsahu a seznamu použité literatury).

Text musí být napsán vhodným textovým editorem počítače po jedné straně bílého neleského papíru formátu A4 při respektování následující doporučené úpravy - písmo Times New Roman 12b; řádkování 1,5; okraje – horní, dolní – 2,5 cm, levý – 3 cm, pravý 2 cm. Fotografie, schémata, obrázky, tabulky musí být očíslovány a musí na ně být v textu poukázáno. Budou zařazeny průběžně v textu, pouze je-li to nezbytně nutné, jako přílohy (viz ad 10).

Odborná terminologie práce musí odpovídat platným normám. Všechny výpočty musí být přehledně uspořádány tak, aby každý odborník byl schopen přezkoušet jejich správnost. Matematické vzorce musí být číslovány (v kulatých závorkách). U vzorců, údajů a hodnot převzatých z odborné literatury nebo z praxe musí být uveden jejich pramen - u literatury citován číselným odkazem (v hranatých závorkách) na seznam použité literatury. Nedostatky ve způsobu vyjadřování, nedostatky gramatické, neopravené chyby v textu mohou snížit klasifikaci práce.

ad 9) BP bude obsahovat alespoň 10 literárních odkazů, z toho nejméně 3 v některém ze světových jazyků. Seznam použité literatury se píše na zvláštním listě. Citaci literatury je nutno uvádět důsledně v souladu s ČSN ISO 690. Na práce uvedené v seznamu použité literatury musí být uveden odkaz v textu BP.

ad 10) Přílohy budou obsahovat jen ty části (speciální výpočty, zdrojové texty programů aj.), které nelze vhodně včlenit do vlastní textové části, např. z důvodu ztráty srozumitelnosti.

III.

Bakalářskou práci student odevzdá ve dvou knihařsky svázaných vyhotoveních, pokud katedra garantující studijní obor neurčí jiný počet. Vnější desky budou označeny takto:

nahoře: *Vysoká škola báňská - Technická univerzita Ostrava*

uprostřed: *BAKALÁŘSKÁ PRÁCE*

dole: *Rok* *Jméno a příjmení*

Kromě těchto dvou knihařsky svázaných výtisků odevzdá student kompletní práci také v elektronické formě do IS EDISON. Práce vložená v elektronické formě do IS EDISON se musí zcela shodovat s prací odevzdanou v tištěné formě. Po vložení BP do IS EDISON bude provedena její kontrola na plagiátorství.

IV.

Nesplnění výše uvedených zásad pro vypracování bakalářské práce může být důvodem nepřijetí práce k obhajobě. O nepřijetí práce k obhajobě rozhoduje v tomto případě garant příslušného studijního oboru. Tyto zásady jsou závazné pro studenty bakalářského studijního programu Nanotechnologie Vysoké školy báňské – Technické univerzity Ostrava od akademického roku 2019/2020.

Ostrava 25. 11. 2019

Ing. Zdeňka Chmelíková, Ph.D.
prorektorka pro studium
VŠB-TU Ostrava

Prohlašuji, že jsem tuto bakalářskou práci vypracoval samostatně. Uvedl jsem všechny literární prameny a publikace, ze kterých jsem čerpal.

Ostrava, 5. června 2020 .....

Prohlášení o využití výsledků práce

- Byl jsem seznámen s tím, že na moji bakalářskou práci se plně vztahuje zákon č. 121/2000Sb., autorský zákon, zejména §35 – užití díla v rámci občanských a náboženských obřadů, v rámci školních představení a užití díla školního a §60 – školní dílo.
- Beru na vědomí, že Vysoká škola báňská – Technická univerzita Ostrava (dále jen VŠB-TUO) má právo nevýdělečně ke své vnitřní potřebě bakalářskou práci užít (§35 odst. 3).
- Souhlasím s tím, že bakalářská práce bude v elektronické podobě uložena v Ústřední knihovně VŠB-TUO k nahlédnutí a jeden výtisk bude uložen u vedoucího bakalářské práce. Souhlasím s tím, že údaje o bakalářské práci budou zveřejněny v informačním systému VŠB-TUO.
- Bylo sjednáno, že s VŠB-TUO, v případě zájmu z její strany, uzavřu licenční smlouvu s oprávněním užít dílo v rozsahu §12 odst. 4 autorského zákona.
- Bylo sjednáno, že užít své dílo - bakalářskou práci - nebo poskytnout licenci k jejímu využití mohu jen se souhlasem VŠB-TUO, která je oprávněna v takovém případě ode mne požadovat přiměřený příspěvek na úhradu nákladů, které byly VŠB-TUO na vytvoření díla vynaloženy (až do jejich skutečné výše).
- Beru na vědomí, že odevzdáním své práce souhlasím se zveřejněním své práce podle zákona č. 111/1998 Sb., o vysokých školách a o změně a doplnění dalších zákonů (zákon o vysokých školách), ve znění pozdějších předpisů, bez ohledu na výsledek její obhajoby.

Jakub Oprštěný, Sokolská třída 2441/38, 702 00 Ostrava

Ostrava, 5. června 2020 .....

I wish to express my sincere thanks to Dominik Legut, Lukáš Kývala, Andrzej Kądzielawa, Sergiu Arapan and Pablo Nieves Cordones for sharing their expertise, and valuable guidence and encouragement extended to me.

Abstrakt

Elektronické, strukturní, magnetické a termodynamické vlastnosti seskvikarbidů uranu a thoria (U_2C_3 a Th_2C_3) byly studovány prostřednictvím výpočtů z prvních principů, se zvláštní pozorností věnovanou vlivu $5f$ elektronů. Použité modely zahrnovaly různé aproximace výměnně-korelační energie, spin orbitální interakci (se značným efektem na U_2C_3 a zanedbatelným vlivem na Th_2C_3) a Hubbard U model pro elektronovou Coulombickou interakci. Míra vlivu těchto efektů je demonstrována přímým srovnáním různých fyzikálních vlastností, jako například pásová struktura, slučovací entalpie, magnetické uspořádání, tepelní kapacita, elastické konstanty, apod. a s experimentálními daty.

Klíčová slova: ab initio; výpočty z prvních principů; seskvikarbid uranu; seskvikarbid thoria; mechanika; termodynamika; fonony

Abstract

Electronic, structural, mechanical, magnetic and thermodynamical properties of uranium and thorium sesquicarbides (U_2C_3 and Th_2C_3) were investigated by the means of first principles calculations, with special interest in the effects of $5f$ electrons. Utilized models included various approximations of exchange-correlation electronic terms, spin-orbital interaction (with a major effect on U_2C_3 and negligible effect on Th_2C_3) and Hubbard U model for electronic Coulomb interaction. The magnitude of these effects is demonstrated on the direct comparison of various physical quantities, such as band structure, enthalpy of formation, magnetic ordering, heat capacity, elastic constants, etc. and compared with experimental data.

Keywords: ab initio; first principles calculations; uranium sesquicarbide; thorium sesquicarbide; mechanics; thermodynamics; phonons

Contents

List of Abbreviations

APW	— Augmented Plane Wave method
DFT	— Density Functional Theory
DOS	— Density of States
GGA	— Generalized Gradient Approximation
LDA	— Local Density Approximation
PAW	— Projector Augmented Wave method
PBE	— Perdew-Burke-Ernzerhof exchange correlation functional
SOI	— Spin-Orbit Interaction
VASP	— Vienna Ab-initio Simulation Package

List of Figures

List of Tables

1 Introduction

1.1 Actinides

Actinides are the chemical elements located in the 7^{th} period with the valence electrons in the f-block of the periodic table. They have 15 members in total (from actinium to lawrencium) and include the heaviest naturally occurring elements, the heaviest one being the uranium. Their ground-state electronic configuration, based on the last preceding noble gas, radon, with valence electrons filling the $5f$, $6p$ and $7s$ orbitals [1]. Actinides have several unique properties [2], such as

- elements heavier than uranium are of artificial origin
- all of their isotopes are radioactive
- they have very large ionic radii
- in compounds and solutions they assume the form of cations
- many often have a large number of oxidation states
- with growing atomic number, the $5f$ electrons tend to be less itinerant
- relativistic and spin-orbit effects play an important role in their chemical properties.

1.1.1 Thorium

Thorium is a silvery metal of face-centered cubic structure (space group No. 225), which transforms into a body-centered phase at higher temperatures. It is a paramagnetic material that is superconducting at low temperatures.

It is chemically very active, forming hydrides, hydroxides, borides, silicides, oxides, carbides and other compounds. There are also many thorium alloys, such as those with iron, cobalt, nickel, tungsten, aluminum and other [2].

1.1.2 Uranium

Uranium has three crystalline phases, with the room-temperature phase being orthorhombic (space group No. 63) and showing an anisotropic thermal expansion, transforming into the tetragonal and body-centered cubic phases with increasing temperature. All of its phases exhibit weak paramagnetism. It has $5f^3$ electrons in its valence orbital.

Its chemical reactivity is very high, as it easily reacts with virtually all elements except noble gases. It corrodes even at room temperature and it often forms non-stoichiometric compounds [2].

1.2 Carbides

Carbides are a large group of chemicals, which are formed by carbon reacting with a more electropositive element. There are three forms of binary carbon compounds, ionic, covalent and interstitial carbides. The last group contains isolated carbon atoms, dimers, etc., like carbon atoms in Th_2C_3 and U_2C_3, which form the so-called C_2 dumbbells. Many of them possess high hardness, like in the case of tungsten carbide, one of the hardest compounds [3].

According to the phase diagrams [2, 4, 5, 6, 7] there exists a number of actinide carbides, from monocarbides, over dicarbides to sesquicarbides of actinide elements. Recently the monocarbide of UC and ThC were studied theoretically [8, 9].

2 Motivation

Interestingly, almost no theoretical predictions were made regarding the structure and properties of U_2C_3 and Th_2C_3. There is only one theoretical study investigating stability and elasticity of U_2C_3 [10] while there is none regarding the structure of Th_2C_3 and only one experimental paper regarding its structure [11]. This work deals with Th_2C_3 synthesized under high pressure and increased temperature with none of its properties measured apart from its space group and lattice parameter. There are much more experimental data available regarding U_2C_3 including its structure and thermal properties. However, the correlation effects for f electrons are expected to be stronger. As U_2C_3 is such a case, having more f electrons, the electronic structure calculations are expected to be much more computationally demanding.

The mail goals of this thesis are to find out the electronic structure of U_2C_3 and Th_2C_3, their phase stability and magnetic ordering, whether there is a noticeable effect of spin-orbit interaction (SOI) on their electronic structure and what are the electronic and thermal properties of the phases (lattice dynamics).

3 Theory

3.1 Density Functional Theory

In this section, we first unveil the Schrödinger many-body equation and all of its potentials (3.1.1), following with the description of commonly used approximations, such as Born-Oppenheimer (3.1.2), Hartree (3.1.3) and Hartree-Fock (3.1.4). Next the energy-to-density mapping by Kohn-Sham-Hohenberg theorem (3.1.5), the necessity of the exchange-correlation energy (3.1.6) and most common basis functions (3.1.7) are described. A part dedicated to the Hubbard U correlation (3.1.8) ends the section.

Observable properties of all matter can be determined from quantum mechanics from the motion of the electrons and the nuclei by solving a many-body Schrödinger equation.

At first, we calculate the electronic structure to find out the ground state of the phase. After having it, we can determine equilibrium properties, such as thermodynamic, mechanical and other. However, due to the difficulty of solving the full many-body equation, many approximations are always applied [12].

3.1.1 Schrödinger Many-Body Equation

In order to describe materials properties, we solve the Schrödinger non-relativistic time-dependent many-body equation

$$\hat{H}\Psi(\{\boldsymbol{r}_i\},\{\boldsymbol{R}_\alpha\},t) = i\hbar\frac{\partial\Psi}{\partial t} \tag{1}$$

where $\hat{H}$ is the exact many-body Hamiltonian and the wavefunction Ψ is a function of all of the electronic ($\boldsymbol{r}_i$) and nuclear ($\boldsymbol{R}_\alpha$) positions. A typical solid contains around 10^{24} positively charged ion cores and an order of 10^{25} electrons which are all interacting with each other while moving much slower than the speed of light ($\boldsymbol{v}_i, \boldsymbol{V}_\alpha \ll c$), so the first approximation often applied is to take the Hamiltonian as a sum of only the nonrelativistic kinetic energies and Coulomb interactions

$$\hat{H} = \hat{T}_E + \hat{T}_N + \hat{V}_{EE} + \hat{V}_{NN} + \hat{V}_{EN} \tag{2}$$

where $\hat{T}_E$ is the kinetic energy of the electrons, $\hat{T}_N$ is the kinetic energy of nuclei, $\hat{V}_{EE}$ is the repulsive Coulomb interaction potential energy between the electrons, $\hat{V}_{NN}$ is the repulsive Coulomb interaction potential energy between the nuclei and finally $\hat{V}_{EN}$ is the combined attractive Coulomb interaction potential energy between the electrons and nuclei. These operators

are defined as

$$\hat{T}_E = -\sum_i \frac{\hbar^2}{2m_e}\nabla_i^2 \tag{3}$$

$$\hat{T}_N = -\sum_\alpha \frac{\hbar^2}{2M_\alpha}\nabla_\alpha^2 \tag{4}$$

$$\hat{V}_{EE} = \frac{1}{2}\sum_{i\neq j} \frac{1}{4\pi\varepsilon_0}\frac{e^2}{|\boldsymbol{r}_i - \boldsymbol{r}_j|} \tag{5}$$

$$\hat{V}_{NN} = \frac{1}{2}\sum_{\alpha\neq\beta} \frac{1}{4\pi\varepsilon_0}\frac{Z_\alpha Z_\beta e^2}{|\boldsymbol{R}_\alpha - \boldsymbol{R}_\beta|} \tag{6}$$

$$\hat{V}_{EN} = -\sum_{i,\alpha} \frac{1}{4\pi\varepsilon_0}\frac{Z_\alpha e^2}{|\boldsymbol{r}_i - \boldsymbol{R}_\alpha|} \tag{7}$$

with m_e being the mass on the electron, M_α being the mass of the nuclei at position $\boldsymbol{R}_\alpha$ and Z_α being its charge [13].

This Hamiltonian omits relativistic effects, such as the spin-orbit coupling, magnetic and mass-velocity effects, and other. Also, if we do not consider *all* of the electrons explicitly, we have to adjust the Hamiltonian for the core polarization effects by adding the many-ion interaction terms. Solving this equation even at the most basic conditions (zero thermodynamic temperature, zero pressure etc.) is still impossible due to the sheer amount of possible states the system can be at (2^n, with n being the number of electrons), and therefore we need to apply further approximations [12].

3.1.2 Born-Oppenheimer Approximation

The mass of the nucleus is at least 1800× larger than the mass of its electrons, hence we can assume that the movement of the nucleus causes an immediate movement of the electron in the same direction (in other words, the electron remains static within the frame of reference of the nucleus) while on the other hand the movement of an electron has no effect on the position of the nucleus.

Due to this approximation, we divide the wavefunction for the whole system into the wavefunction depending on the position of electrons (φ) for a fixed position of ions and the one depending only on the position of the ion cores (ψ)

$$\Psi(\{\boldsymbol{r}_i\},\{\boldsymbol{R}_\alpha\}) = \varphi(\{\boldsymbol{r}_i\},\{\boldsymbol{R}_\alpha\})\psi(\{\boldsymbol{R}_\alpha\})e^{-\frac{iEt}{\hbar}} \tag{8}$$

We can substitute this into the Eq. 1 and 2 and derive the Schrödinger equation in electron positions (φ)

$$\left(\hat{T}_E + \hat{V}_{EE} + \hat{V}_{EN}\right)\varphi_n = E_n\varphi_n \tag{9}$$

which can be solved, for a fixed set of ion-core positions $\boldsymbol{R}_\alpha$, for the eigenvalues $E_n(\{\boldsymbol{R}_\alpha\})$ and eigenfunctions $\varphi_n(\{\boldsymbol{r}_i\},\{\boldsymbol{R}_\alpha\})$.

We can then derive the Schrödinger equation in nuclear positions (ψ)

$$\left(\hat{T}_N + \hat{V}_{NN} + E_n(\boldsymbol{R}_\alpha)\right)\psi_{n,\lambda} = E_{n,\lambda}\psi_{n,\lambda} \tag{10}$$

which includes the electronic positions in the term $E_n(\{\boldsymbol{R}_\alpha\})$ in the potential energy, which was derived using Eq. 9. In this way, we are able to get different eigenvalues $E_{n,\lambda}$ and eigenfunctions $\psi_{n,\lambda}(\{\boldsymbol{R}_\alpha\})$, because each value of n results in a different potential energy from Eq. 9.

3.1.3 Hartree Approximation

In order to make the solution to the electronic Schrödinger equation more feasible, we can reduce the electronic wavefunction φ into a product of wavefunctions ϕ for every single electron (whose total amount goes up to n)

$$\varphi(\{\boldsymbol{r}_i\}) = \phi_1(\boldsymbol{r}_1)\phi_2(\boldsymbol{r}_2)\dots\phi_n(\boldsymbol{r}_n) \tag{11}$$

and we get a single-electron approximation where we consider electrons to be independent of each other. We assume that every electron is influenced by the same potential of an averaged distribution of all other electrons [14]. The Schrödinger equation for each ϕ_i that has been approximated by the Hartree approximation then contains a single set of terms

$$\left(\hat{T}_E + \hat{V}_{Ef} + \hat{V}_{Nf}\right)\phi_i(\boldsymbol{r}_i) = \varepsilon\phi_i(\boldsymbol{r}_i) \tag{12}$$

where the new operators are

$$\hat{V}_{Ef} = \frac{e^2}{4\pi\varepsilon_0}\sum_{j\neq i}\int\frac{|\phi_j(\boldsymbol{r}_j)|^2}{|\boldsymbol{r}_i - \boldsymbol{r_j}|}\mathrm{d}\boldsymbol{r}_j \tag{13}$$

$$\hat{V}_{Nf} = -\frac{e^2}{4\pi\varepsilon_0}\sum_{\alpha}\frac{Z_\alpha}{|\boldsymbol{r}_i - \boldsymbol{R}_\alpha|} \tag{14}$$

where the first term in the Hamiltonian denotes the kinetic energy, second represents the Coulomb potential of other electrons and the last is the attractive Coulomb potential of ion cores.

In this way, the Hartree approximation effectively reduces the Schrödinger equation to a problem of one electron moving independently of all other electrons within the static potential of the lattice (represented by the ionic potential) and the average potential of all the other electrons (representing the electron's interaction with them) [14].

3.1.4 Hartree-Fock Approximation

An n-electron wavefunction φ_i can be obtained if we write out a Slater determinant for a given basis of wavefunctions ϕ_i of n particles

$$\varphi(\{\boldsymbol{r}_i\}) = \frac{1}{\sqrt{n!}}\begin{vmatrix}\phi_1(\boldsymbol{r}_1) & \phi_1(\boldsymbol{r}_2) & \cdots & \phi_1(\boldsymbol{r}_n)\\ \phi_2(\boldsymbol{r}_1) & \phi_2(\boldsymbol{r}_2) & \cdots & \vdots\\ \vdots & \vdots & \ddots & \vdots\\ \phi_n(\boldsymbol{r}_1) & \cdots & \cdots & \phi_n(\boldsymbol{r}_n)\end{vmatrix} \tag{15}$$

and if we minimize the energy of the Hamiltonian from Eq. 9 with respect to variations in the ϕ_i, we get the Hamiltonian in the form of

$$\left(\hat{T}_E + \hat{V}_{Ef} + \hat{V}_{Nf} + \hat{V}_{\text{ex}}\right)\phi_i(\boldsymbol{r}_i) = \varepsilon\phi_i(\boldsymbol{r}_i) \tag{16}$$

with $\hat{V}_{\text{ex}}\phi_i(\boldsymbol{r}_i)$ being the *exchange interaction* (or Fock contribution)

$$\hat{V}_{\text{ex}}\phi_i(\boldsymbol{r}_i) = -\frac{e^2}{4\pi\varepsilon_0}\sum_j \int \frac{\phi_j^*(\boldsymbol{r}_j)\phi_i(\boldsymbol{r}_j)}{|\boldsymbol{r}_i - \boldsymbol{r}_j|}\phi_i(\boldsymbol{r}_i)\mathrm{d}\boldsymbol{r}_j \tag{17}$$

which is a Coulomb term originating from the antisymmetry of the wavefunction 15. This operator takes into account the Pauli exclusion principle, because the spin of j states has to be the same as the one on the i states. Together with the negative sign, it lowers the repulsive Coulomb interaction energy due to the minimization of the spatial wavefunctions' overlap. The term lowers the Coulomb interaction by keeping the electrons with the same spins apart, however, there is no such influence on the electrons with opposite spins, so in the end the tendency towards cohesion is still underestimated. Because of this the *correlation energy*, which includes the effect of this influence, has been defined as the difference between the actual energy of the system and the energy from Hartree-Fock approximation [12, 14].

3.1.5 Kohn-Sham-Hohenberg Theorem

Hohenberg-Kohn theorem [15] states that the total energy of the system depends only on the ground-state electron density, so that the energy is defined as a functional of the electron density

$$E = E[\rho(\boldsymbol{r})] \tag{18}$$

where $\rho(\boldsymbol{r})$ is the electron density. This makes solving the many-body Schrödinger equation much easier because it reduces the required minimization of 2^{3n} degrees of freedom to only 3 of the coordinates of the electron density functional.

The electron density can also be determined from the ion core position

$$E = E[\rho(\boldsymbol{r}, \{\boldsymbol{R}_\alpha\})] \tag{19}$$

with $\{\boldsymbol{R}_\alpha\}$ still represent that the theorem is being applied to every set of fixed ion-core positions [12].

Kohn-Sham theorem [16] introduces an average effective potential V_{eff} for each independently moving electron. This potential represents how the electrons are affected by other electrons and the ion core. For the effective electrons, the Schrödinger equation reads

$$\left(\hat{T}_E + \hat{V}_{eff}\right)\psi_i(\boldsymbol{r}) = \varepsilon_i\psi_i(\boldsymbol{r}) \tag{20}$$

with the effective potential V_{eff} being the sum of Coulomb ($\hat{V}_C$) and exchange-correlation ($\hat{V}_{xc}$) potential

$$\hat{V}_{eff}(\boldsymbol{r}) = \hat{V}_C + \hat{V}_{\text{xc}}[\rho(\boldsymbol{r})] \tag{21}$$

where

$$\hat{V}_C = \frac{e^2}{4\pi\varepsilon_0} \int \frac{\rho(\boldsymbol{r}')}{|\boldsymbol{r} - \boldsymbol{r}'|} \mathrm{d}\boldsymbol{r}' - \hat{V}_{Nf} \tag{22}$$

$$\hat{V}_{xc} = \frac{\partial E_{xc}}{\partial \rho} \tag{23}$$

and E_{xc} is the exchange-correlation energy. The total ground-state energy of the system can then be calculated [13]

$$E_0(\rho) = \int \psi^* \hat{T} \psi \, \mathrm{d}\boldsymbol{r} + \hat{V}_C \rho(\boldsymbol{r}) \mathrm{d}\boldsymbol{r} + E_{xc}[\rho(\boldsymbol{r})] \tag{24}$$

where the first term represents the sum of kinetic energies of effective electrons, second term is the Coulomb potential energy from Eq. 22 and the last term is the exchange-correlation energy which lowers the total energy in a same way (and for the same reasons) as the Fock contribution in Eq. 17.

3.1.6 Exchange-Correlation Energy

No approximations were made during the derivation of previous equations. However, the precise expression for the exchange-correlation energy is unknown. Since the early history of DFT, several approximative functionals that estimate its value were formulated, with each of them being different in their degree of accuracy, computational demands and focus. The two most commonly used ones are the local density approximation (LDA) and the generalized gradient approximation (GGA) [12].

LDA is based on the assumptions of Kohn and Sham [16], where we can assume that local E_{xc} can be calculated as a uniform electron gas

$$E_{xc}^{LDA}[\rho(\boldsymbol{r})] = \int \rho(\boldsymbol{r}) \varepsilon_{xc}^{LDA}[\rho(\boldsymbol{r})] \mathrm{d}\boldsymbol{r} \tag{25}$$

where $\varepsilon_{xc}^{LDA}[\rho(\boldsymbol{r})]$ is the exchange-correlation energy per electron, which represents the interaction of the electron with many-electron system of constant electron density [13, 14]. This approach achieves a very high precision when describing the electron density, solid-state geometry and properties, but is generally a poor choice for the description of inhomogeneous systems due to the resulting errors in binding and cohesive energies [14].

To resolve this, the generalized gradient method using the local *gradient* of the density has been developed [17]

$$E_{xc}^{GGA}[\rho(\boldsymbol{r})] = \int f[\rho(\boldsymbol{r}), \nabla\rho] \mathrm{d}\boldsymbol{r} \tag{26}$$

which takes into account the local differences in the electron density and therefore is more accurate for the treatment of small systems like atoms, molecules and small clusters [12, 14].

3.1.7 Computational Implementation

Various implementations of DFT using LDA and GGA differ mainly in the choice of the basis functions. The two most common approaches are the augmented plane wave (APW) and

pseudopotential methods.

The APW method [18] separates the space into spheres surrounding each atom, where the spheres' radii are different for different elements, and the interstitial region between them. We can then spherically-average the potential with respect to each atomic center in each sphere and volume-average it within the interstitial region. The wavefunctions can be then obtained in polar coordinates as a product of a radial function $R_{nl}(r)$ and spherical harmonics $Y_{lm}(\theta, \phi)$ [12]

$$\psi(\boldsymbol{r}) = R_{nl}(r)Y_{lm}(\theta, \phi) \tag{27}$$

and since the potential has been replaced by a constant, the solutions for the interstitial region are plane waves

$$\psi(\boldsymbol{r}) = e^{i\boldsymbol{k}\cdot\boldsymbol{r}} \tag{28}$$

and these two equations effectively define the basis, where we can represent any potential as their superposition [12].

The pseudopotential methods stem from the fact that core electrons are unimportant for many physical properties, and so the core electrons and nuclei are replaced by a pseudopotential which does not affect the valence shells. The difference is that while the real potential is singular near the nucleus, the pseudopotential is finite at the same location and therefore a lot smoother. Due to this fact, the pseudopotential can be expanded into computationally simplified plane waves.

The advantage of pseudopotential methods are mainly the lower computational demands, since the electrons near the ion core have to be calculated only once and the result can be used during the whole course of the calculation [12].

3.1.8 Hubbard U Correlation

While the DFT provides very accurate results for itinerant systems, it is less accurate for structures with only partly filled valence d and f shells. In metals, electrons tend to be delocalized over the whole crystal. However, in some systems the strength on-site Coulomb energy (the energy cost of putting two electrons on the same lattice site) may prevent the free movement of electrons through the crystal. The itinerant behavior of electrons effectively breaks down due to the high cost of double occupancy of a site, which means that we can no longer treat electrons as free particles, but electron correlations, which take into account the fact that the electrons have to avoid each other if the Coulomb repulsion is too large. This competition between the itinerant and localized behavior (parametrized by U) is described in Hubbard model [19].

The Hubbard model, in a real-space second quantization formalism, is capable to describe the electrons localized at atomic orbitals, and is written as

$$\hat{H}_{Hub} = t \sum_{\langle i,j\rangle,\sigma} \left(c^{\dagger}_{i,\sigma} c_{j,\sigma} + h.c. \right) + U \sum_{i} n_{i,\uparrow} n_{i,\downarrow} \tag{29}$$

where $\langle i, j\rangle$ denotes nearest-neighbor atomic sites, $c^{\dagger}_{i,\sigma}, c_{j,\sigma}$ are electronic creation, annihilation and $n_{i,\sigma}$ are operators corresponding to electrons of spin σ on site i.

The first term of the Hubbard Hamiltonian describes the "hopping" of strongly localized

electrons from one atomic site to its neighbors whose amplitude t corresponds one-to-one with the dispersion relation (the electronic bands) of the valence electronic states and represents the single-particle term of the total energy [20].

The second term of the equation is the product of the occupation numbers of atomic states on the same site, which has a magnitude U (the so called Hubbard U) and represents the Coulomb repulsion for the electrons *on the same site*, due to the strong localization [20].

The balance between t and U controls the behavior of the whole system and the character of their electronic ground state. If U is *larger* than t, we get an insulating character of the ground state, because the single-particle terms of the energy, minimized by electronic delocalization on more extended states, are overcome by short-range Coulomb interactions (the energy cost of double occupancy of the same site). The system therefore becomes an insulator when the electrons do not have sufficient energy to overcome the repulsion of neighboring sites (they cannot "hop"). If U is *smaller* than t, we get a metallic behavior of the system.

The DFT functional is corrected by using the Hubbard Hamiltonian from Eq. 29 to describe "strongly correlated" electronic states, such as localized d or f orbitals, while the rest of the valence electrons are treated within the standard level of approximation. The total energy of a system obtained through the DFT+U approach can be written as

$$E_{DFT+U}[\rho(r)] = E_{DFT}[\rho(r)] + E_{Hub}[\{n^{I\sigma}_{mm'}\}] - E_{dc}[n^{I\sigma}] \tag{30}$$

where the term E_{Hub} represents the electron-electron interactions modelled by the Hubbard Hamiltonian. The so called "double counting" (dc) term E_{dc}, which models the energy from correlated electrons as a mean-filed approximation to E_{Hub}, is introduced to subtract the interaction energy already present in E_{Hub} from the total energy obtained through the standard DFT approach E_{DFT} and thus avoid its double-counting.

In practice, the value of U is usually determined semiempirically.. This is needed due to the fact the required scale of the Hubbard U correlation to the total energy functional is originally unknown because it depends not only on the type of the element but also on its position in the crystal lattice, the structural and magnetic properties of crystal and many other [20].

3.2 Crystalline Solids

This subsection deals with the definitions of primitive cell (3.2.2), Bravais lattice (3.2.1), then we define the most widely used primitive lattice, the Wigner-Seitz lattice (3.2.4), after that we take a look at the reciprocal lattice (3.2.3), and the resulting Bloch theorem (3.2.5).

3.2.1 Bravais Lattice

A Bravais lattice is an infinite array of discrete points which are arranged and oriented in a way so that it always appears exactly the same, from whichever of the points the array is viewed [22]. Their position vectors are are written as

$$\boldsymbol{R} = n_1\boldsymbol{a}_1 + n_2\boldsymbol{a}_2 + n_3\boldsymbol{a}_3 \tag{31}$$

where n_1, n_2 and n_3 index a particular unit cell in space, and range through all integral values [22], and $\boldsymbol{a}_1$, $\boldsymbol{a}_2$ and $\boldsymbol{a}_3$ are primitive (translation) vectors in three dimensional space that generate the lattice [21].

3.2.2 Primitive Cell

All of the naturally occurring elements can, under certain conditions, crystallize in a one of the crystal structures, as can majority of condensed systems. Ideal crystal is then composed of infinite repeats of identical structural units in all dimensions called the unit cell. The smallest possible unit cell, that is the one occupying the smallest possible volume, is called the primitive cell. Its volume is defined as

$$V_c = \boldsymbol{a}_1 \times \boldsymbol{a}_2 \cdot \boldsymbol{a}_3 \tag{32}$$

The unit cell may contain more then one atom, in which case the crystal structure is determined through the addition of the basis to every lattice point, which allows us to build the space lattice [21].

3.2.3 Reciprocal Lattice

Reciprocal lattice [22], which is an inversion of the real lattice, is very often used to describe the behavior of electrons in a crystal lattice. For three dimensional space, its primitive vectors are

$$\boldsymbol{b}_1 = 2\pi \frac{\boldsymbol{a}_2 \times \boldsymbol{a}_3}{\boldsymbol{a}_1 \times \boldsymbol{a}_2 \cdot \boldsymbol{a}_3} \tag{33}$$

$$\boldsymbol{b}_2 = 2\pi \frac{\boldsymbol{a}_3 \times \boldsymbol{a}_1}{\boldsymbol{a}_1 \times \boldsymbol{a}_2 \cdot \boldsymbol{a}_3} \tag{34}$$

$$\boldsymbol{b}_3 = 2\pi \frac{\boldsymbol{a}_1 \times \boldsymbol{a}_2}{\boldsymbol{a}_1 \times \boldsymbol{a}_2 \cdot \boldsymbol{a}_3} \tag{35}$$

which can be verified by the fact that $\boldsymbol{b}_i$ satisfies the equality

$$\boldsymbol{b}_i \boldsymbol{a}_j = 2\pi \delta_{ij} \tag{36}$$

where δ_{ij} is the Kronecker delta

$$\delta_{ij} = 0, \quad i \neq j \tag{37}$$

$$\delta_{ij} = 1, \quad i = j \tag{38}$$

The cell volume of a reciprocal lattice is defined in the same way as in Eq. 32

$$\boldsymbol{b}_1 \times \boldsymbol{b}_2 \cdot \boldsymbol{b}_3 = \frac{(2\pi)^3}{\boldsymbol{a}_1 \times \boldsymbol{a}_2 \cdot \boldsymbol{a}_3} \tag{39}$$

Translation vector for the reciprocal lattice $\boldsymbol{G}$ can be written in the same way as in the Eq. 31

$$\boldsymbol{G} = k_1 \boldsymbol{b}_1 + k_2 \boldsymbol{b}_2 + k_3 \boldsymbol{b}_3 \tag{40}$$

3.2.4 Primitive Cell in Reciprocal Space

One of the most commonly used primitive cells is the primitive cell in reciprocal space, so-called Wigner-Seitz cell. It can be constructed by drawing lines to connect a lattice point to all of its neighboring points and drawing new planes at the midpoint and normal to them. The smallest volume enclosed in this way is the Wigner-Seitz *primitive* cell [21].

3.2.5 Bloch Theorem

From Eq. 31 and 40 follows that

$$\boldsymbol{G} \cdot \boldsymbol{R} = 2\pi(k_1 n_1 + k_2 n_2 + k_3 n_3) \tag{41}$$

and we can also write the relationship between Bravais lattice vectors and reciprocal lattice vectors as

$$e^{i\boldsymbol{G}\cdot\boldsymbol{R}} = 1 \tag{42}$$

and its Fourier transform for the periodic system of Bravais lattice is written in a form of

$$f(\boldsymbol{r}) = \sum_{G} e^{i\boldsymbol{G}\cdot\boldsymbol{R}} f(\boldsymbol{G}) \tag{43}$$

with $f(\boldsymbol{G})$ denoting the Fourier transform components [22].

This results into the definition of Bloch theorem, which states that [23] *eigenstates of the translation operators vary from one cell to another in the crystal with the phase factor given in*

$$\psi(\boldsymbol{r} + \boldsymbol{R}) = e^{i\boldsymbol{G}\cdot\boldsymbol{R}} \psi(\boldsymbol{r}) \tag{44}$$

or in other words that the single-particle wavefunction reaches the same value in every equivalent position in the lattice, and that its Hamiltonian has a translational periodicity of the Bravais lattice.

3.3 Elastic Properties

In this part, we first show the derivation of the elastic coefficients from Hooke's law (3.3.1), following with the derivation of the adiabatic elastic coefficients from the 1st law of thermodynamics (3.3.2) and then we derive the elastic constants (3.3.3), such as bulk, shear and Young's modulus from previously derived parameters, and describe their relationships (3.3.4) and a way of judging materials isotropicity with Cauchy pressure and its ductility with Poisson's and Pugh's ratio.

3.3.1 Elastic Coefficients

Single crystal's properties are described by the elastic stiffness coefficients c_{ij} and elasticity, which is considered to be a special case of long-wavelength lattice vibrations.

The relationship between the elastic strain ε_{kl} and stress σ_{ij} is described by the Hooke's law

$$\sigma_{ij} = \sum_{k,l=1}^{3} c_{ijkl}\varepsilon_{kl} \tag{45}$$

where the indeces i, j, k and l run from 1 to 3 and so the materials properties are described by a fourth order elasticity tensor with $3^4 = 81$ elements of ε_{ijkl}. Because of the symmetricality of the $c_{ijkl} = c_{klij} = c_{jikl} = c_{ijlk}$, the number of ε_{ijkl} elements is reduced to at most 21. These can further be arranged in a 6×6 symmetric matrix that can be contracted to a matrix of at most 6 elements as described in the Voigt's contraction scheme in Tab. 1. Given this fact, the Hooke's law from Eq. 45 can be rewritten into a simpler form

$$\sigma_\alpha = \sum_{\beta=1}^{6} c_{\alpha\beta}\varepsilon_\beta \tag{46}$$

where

$$\sigma_\alpha = \sigma_{ij}; \quad \varepsilon_\beta = \varepsilon_{kl} \text{ if } \beta = 1, 2 \text{ or } 3; \quad \varepsilon_\beta = 2\varepsilon_{kl} \text{ if } \beta = 4, 5 \text{ or } 6 \tag{47}$$

i, j or k, l	11	22	33	23 or 32	13 or 31	12 or 21
α or β	1	2	3	4	5	6

Table 1: Voigt's contraction scheme

With cubic lattice, we can apply the following symmetry [14]

$$c_{11} = c_{22} = c_{33}; \quad c_{12} = c_{13} = c_{23}; \quad c_{44} = c_{55} = c_{66} \tag{48}$$

so the resulting matrix has the following form

$$c_{\text{cubic}} = \begin{pmatrix} c_{11} & c_{12} & c_{12} & 0 & 0 & 0 \\ c_{12} & c_{11} & c_{12} & 0 & 0 & 0 \\ c_{12} & c_{12} & c_{11} & 0 & 0 & 0 \\ 0 & 0 & 0 & c_{44} & 0 & 0 \\ 0 & 0 & 0 & 0 & c_{44} & 0 \\ 0 & 0 & 0 & 0 & 0 & c_{44} \end{pmatrix} \tag{49}$$

with 3 independent elastic constants (c_{11}, c_{12} and c_{44}). However, there are also special lattice structures that may require 7 elastic constants to be described [24].

3.3.2 Adiabatic Elastic Coefficients

In order to get an insight upon the influence of pressure, temperature and other variables, we can express $c_{\alpha\beta}$ as derivatives of thermodynamic functions [24]. We can take the first law of thermodynamics

$$\mathrm{d}U = T\mathrm{d}S - p\mathrm{d}V \tag{50}$$

where U represents internal energy, T is thermodynamic temperature, S is entropy, p is pressure and V is volume, and resolve the forces and deformations into Cartesian components (with positive stress of lattice corresponding to a negative pressure within the system)

$$\mathrm{d}U = T\mathrm{d}S + V_0 \sum_{i=1}^{6} \sigma_i \mathrm{d}\varepsilon_i \tag{51}$$

Then we can get the components of the stress tensor for an adiabatic deformation (with no change of heat within the volume V_0)

$$\sigma_i = \frac{1}{V_0} \left(\frac{\partial U}{\partial \varepsilon_i} \right)_{S,\varepsilon'} \tag{52}$$

with the subscripts S and ε' denoting that the entropy and all the $\varepsilon_i \neq \varepsilon_j$ are held constant and the prefactor $1/V_0$ keeping the σ_i independent of the size of the system.

Similarly we can get the components $c_{\alpha\beta}$ of the stiffness tensor

$$c_{(\alpha\beta)S} = \left(\frac{\partial \sigma_\alpha}{\partial \varepsilon_\beta} \right)_{S,\varepsilon'} = \frac{1}{V_0} \left(\frac{\partial^2 U}{\partial \varepsilon_\alpha \partial \varepsilon_\beta} \right)_{S,\varepsilon'} \tag{53}$$

where S and all ε are kept constant except ε_α and ε_β.

In order to achieve even higher precision, we can calculate the higher-order elastic constants. We can rewrite the energy of a crystal into a Taylor series in powers of the strain ε_i

$$U = U(\varepsilon_i = 0) + V_0 \sum c_i \varepsilon_i + \frac{1}{2} V_0 \sum c_{ij} \varepsilon_i \varepsilon_j + \frac{1}{6} V_0 \sum c_{ijk} \varepsilon_i \varepsilon_j \varepsilon_k + \cdots \tag{54}$$

where indices i, j, k go from 1 to 6. And if we now take into account only the first three terms, we get the definition of the *third-order* adiabatic elastic coefficients

$$(c_{ijk})_S = \frac{1}{V_0} \left(\frac{\partial^3 U}{\partial \varepsilon_i \partial \varepsilon_j \partial \varepsilon_k} \right)_{S,\varepsilon'} \tag{55}$$

To conclude previous derivations, it is possible to calculate the elastic constants from either stress–strain or energy–strain relationships.

3.3.3 Elastic Moduli

Both one- and multiphase polycrystalline systems' elastic parameters can be represented by the bulk B, shear G and Young's E moduli.

Bulk modulus B is a measure of materials resistance to compression. It is an isotropic quantity that can be derived either from elastic constants [24] as

$$B = \frac{c_{11} + 2c_{12}}{3} \tag{56}$$

or from a first derivative of pressure with respect to volume, which can be rewritten into second derivative of energy [21]

$$B = -V \frac{\mathrm{d}p}{\mathrm{d}V} = V \frac{\mathrm{d}U^2}{\mathrm{d}V^2} \tag{57}$$

and so we are able to derive bulk modulus from the energy–volume curve.

Shear modulus G is a measure of materials resistance to shear stress. For a cubic isotropic system it is defined as

$$G = c_{44} \tag{58}$$

where the elastic constant c_{44} is tetragonal deformation.

Young's modulus E is used to describe materials resistance to uniaxial deformation and for the case of elastically isotropic material [24] is defined as

$$E = \frac{(c_{11} - c_{12})(c_{11} + 2c_{12})}{c_{11} + c_{12}} \tag{59}$$

3.3.4 Elastic Coefficients and Moduli Relationships

Relationships between elastic constants are used as one of the metrics to judge the static stability of a structure. For a cubic system, this is described by Born's elastic stability condition [24]

$$c_{11} > |c_{12}|; \quad c_{11} + 2c_{12} > 0; \quad c_{44} > 0 \tag{60}$$

Elastic constants also define Cauchy pressure, which is used as a measure of materials mechanical isotropicity [24]

$$P_c = c_{12} - c_{44} \tag{61}$$

where the higher Cauchy pressure corresponds to higher anisotropicity, in other words if $c_{12} = c_{44}$, then the material is isotropic.

Zener anisotropy A_Z is another way to measure crystals anisotropy

$$A_Z = \frac{c_{44}}{C'} \tag{62}$$

where the C' is Zener's elastic constant

$$C' = \frac{c_{11} - c_{12}}{2} \tag{63}$$

and can tell us whether the material is isotropic ($A_Z = 1$) or not [24]. Poisson's ratio ν can be used as a measure of materials ductility and brittleness in the cases when we are comparing two similar structures. It can be defined using elastic constants as

$$\nu = \frac{c_{12}}{c_{11} + c_{12}} \tag{64}$$

Poisson's ratio can also be used as a factor to translate one elastic modulus into another [24]

$$\nu = \frac{3B - 2G}{2(3K + G)} = \frac{E}{2G} - 1 = \frac{1}{2} - \frac{E}{6B} \tag{65}$$

Similarly as Poisson's ratio ν, Pugh's ratio G/B can also be used to describe the ductility of similar structures (due to the fact described in previous paragraph) with brittle to ductile border at 0.57, where material with lower Pugh ratio is more ductile while higher Pugh ratio means increased brittleness [25].

3.4 Lattice Dynamics

The last section of the theoretical part is devoted to lattice vibrations (phonons) and their treatment through the harmonic approximation (3.4.1) and its energy contribution (3.4.2). Several thermodynamic properties from the harmonic (3.4.3) approximation are described.

Atoms in their equilibrium positions in the crystal lattice vibrate with an amplitude dependent on the temperature. Thanks to the existence of crystal symmetry, we are able to study these thermal vibrations in terms of collective motion of the ionic modes called phonons. These can be excited and populated like electronic states, but since phonons are bosons and not fermions like electrons, they do not obey the Pauli exclusion principle (one state can be occupied by more than two phonons) nor is their total number fixed. This is due to the fact that vibrations can be arbitrarily excited by simply heating the solid [26].

The description of phonons is based around two basic assumptions:

1. Despite the ionic motion, the Bravais lattice is preserved in a form of an average ionic configuration.

2. Ionic displacement due to the vibration is small compared with its distance from other ions.

The first assumption allows us to write the position of a displaced ion $\boldsymbol{R}$ as

$$\boldsymbol{R} = \boldsymbol{R}_0 + \boldsymbol{u} \tag{66}$$

with $\boldsymbol{R}_0$ being the ion's equilibrium position and $\boldsymbol{u}$ being its the displacement.

The ionic Hamiltonian can be described as a sum of kinetic energy and ionic potential Φ, which can be written simply as

$$\Phi = \Phi_0(\boldsymbol{R}_{0,l\kappa,\ldots}) + \Phi'(\boldsymbol{u}_{l\kappa,\ldots}) \tag{67}$$

with l denoting the particular unit cell and κ atoms in each unit cell.

3.4.1 Harmonic Approximation

The kinetic energy contribution K of a single ion to the total energy is

$$K = \frac{1}{2} M_\kappa \left(\frac{\mathrm{d}\boldsymbol{u}_{l\kappa}}{\mathrm{d}t} \right)^2 \tag{68}$$

where the M_κ denotes weight of the atom [27].

Crystal potential energy Φ as a function of the ionic displacements can be expanded as a

Taylor series

$$\begin{aligned}\Phi =&\Phi_0 + \sum_{l\kappa}\sum_{\alpha}\Phi_\alpha(l\kappa)\boldsymbol{u}_\alpha(l\kappa)\\ &+\frac{1}{2!}\sum_{ll'\kappa\kappa'}\sum_{\alpha\beta}\Phi_{\alpha\beta}(l\kappa,l'\kappa')\boldsymbol{u}_\alpha(l\kappa)\boldsymbol{u}_\beta(l'\kappa')\\ &+\frac{1}{3!}\sum_{ll'l''\kappa\kappa'\kappa''}\sum_{\alpha\beta\gamma}(l\kappa,l'\kappa',l''\kappa'')\times\boldsymbol{u}_\alpha(l\kappa)\boldsymbol{u}_\beta(l'\kappa')\boldsymbol{u}_\gamma(l''\kappa'')+\cdots\end{aligned} \tag{69}$$

where α, β, ... are Cartesian indices and Φ_0, $\Phi_\alpha(l\kappa)$, $\Phi_{\alpha\beta}(l\kappa,l'\kappa')$ and $\Phi_{\alpha\beta\gamma}(l\kappa,l'\kappa',l''\kappa'')$ represent the zeroth, first, second, and third order force constants, respectively. In harmonic approximation (for smaller displacements at constant volume), we utilize only second-order terms [28]. As the zeroth term is an arbitrary constant (set to zero for convenience), and first order term corresponds to the equilibrium state at zero temperature (also zero contribution to energy), or minimum in the total energy, and third order and higher terms are needed for anharmonic effects only [26].

We can therefore write the sum of the kinetic energy of a single ion and its *harmonic potential* (also known as *quadratic*) as

$$H'[\boldsymbol{u}(l\kappa)] = K + \Phi(2) \tag{70}$$

with $\Phi(2)$ denoting the use of only the second-order term of the crystal potential energy [27].

The second-order force constants $\Phi_{\alpha\beta}(l\kappa,l'\kappa')$ can then be derived either from the ionic potential or as a derivative of a force $F_\alpha(l\kappa) = -\frac{\partial\Phi}{\partial\boldsymbol{u}_\alpha(l\kappa)}$ as

$$\Phi_{\alpha\beta}(l\kappa,l'\kappa') = \frac{\partial^2\Phi}{\partial\boldsymbol{u}_\alpha(l\kappa)\partial\boldsymbol{u}_\beta(l'\kappa')} = \frac{\partial F_\beta(l'\kappa')}{\partial\boldsymbol{u}_\alpha(l\kappa)} \tag{71}$$

and are acting upon nearby ions. These forces include the repulsive Coulomb interaction of ion cores and indirect interaction mediated by electrons, and result from the change of the electron density due to the movement of ion cores [27, 28].

Translation symmetry of the force constants $\Phi(l\kappa,l'\kappa')$ tells us that the wavefunctions are plane waves. Those can be, with a displacement κ of an ion in a unit cell l, written as

$$\boldsymbol{u}_{l\kappa}(\boldsymbol{q},\omega) = \boldsymbol{u}_{0\kappa}e^{i(\boldsymbol{q}\cdot R_l-\omega t)} \tag{72}$$

with $\boldsymbol{q}$ being the wavevector, ω the frequency of the wave and R_l denoting the position of the ion in l-th unit cell.

Wavevector $\boldsymbol{q}$ and frequency of the propagating wave ω can be used to determine several materials properties. If we substitute the Eq. 72 into 70 and resolve through the Newton's second law ($m\boldsymbol{a} = \boldsymbol{F}$, where the acceleration is the second time derivative of the displacement $\boldsymbol{u}$) and take the Fourier transform of the force constants, we get a dynamic matrix, which can be rewritten into the ω as a function of q, which is the so-called dispersion relation. This dispersion relation, and the resulting dispersion law, binds together wavevector $\boldsymbol{q}$ and frequency ω, whose relationship allows us (for the propagation in one dimension, where q is the wavenumber) to

define

$$v_0 \equiv \lim_{q \to 0^+} \frac{\omega}{q} \tag{73}$$

$$v_f \equiv \frac{\omega}{q} \tag{74}$$

$$v_g \equiv \frac{\mathrm{d}\omega}{\mathrm{d}q} \tag{75}$$

where v_0 is the long wave limit, or the speed of sound in the material, v_f is phase velocity, or the speed of the propagating wave, and v_g is group velocity, or speed of the flow of energy [27].

3.4.2 Energy of Lattice Vibrations

The number of phonons of frequency ω at a given temperature follows the Bose-Einstein distribution

$$n = \frac{1}{e^{(\hbar\omega)/(k_B T)} - 1} \tag{76}$$

where k_B is the Boltzmann constant and $\hbar$ is the reduced Planck constant [27].

Energy of a phonon mode with a given frequency ω is

$$E = \left(n + \frac{1}{2}\right)\hbar\omega \tag{77}$$

with $\frac{1}{2}\hbar\omega$ being the energy of vibrations at zero temperature [27].

The total energy of phonon excitations then is its sum

$$E = \sum_i \left(n + \frac{1}{2}\right)\hbar\omega_i \tag{78}$$

where i indexes that the sum is taken over all phonon bands [28].

3.4.3 Thermodynamic Properties at Constant Volume

Once we know the previously derived quantities, we are able to derive several thermodynamic properties at constant volume [29], such as heat capacity

$$C_V = \left(\frac{\partial E}{\partial T}\right)_V = \sum_i C_i = \sum_i \left(\frac{\hbar\omega_i}{k_B T}\right)^2 \frac{e^{(\hbar\omega/k_B T)}}{\left[e^{(\hbar\omega/k_B T)} - 1\right]^2} \tag{79}$$

phonon free energy at constant volume (the Helmholtz free energy)

$$F_{ph} = \Phi + \frac{1}{2}\sum_i \hbar\omega_i + k_B T \sum_i \ln\left[1 - e^{(-\hbar\omega_i/k_B T)}\right] \tag{80}$$

where Φ represents the potential energy of the crystal, and entropy

$$S = -\left(\frac{\partial F}{\partial T}\right)_V = \frac{1}{2T}\sum_i \hbar\omega_i \coth\left(\frac{\hbar\omega_i}{2k_B T}\right) - k_B \sum_i \ln\left[2\sinh\left(\frac{\hbar\omega_i}{2k_B T}\right)\right] \tag{81}$$

3.4.4 Electron Heat Capacity

Classical statistical physics states that a free particle should have a heat capacity equal to $\frac{3}{2}k_B$, the contribution to the heat capacity of electron gas of N freely moving atoms with one contributing valence electron then $\frac{3}{2}Nk_B$. However, experimental observations at room temperature revealed that it is actually less than one hundredth of this amount.

When the atom is heated up, its electrons may absorb enough energy to jump into higher excitation states (with higher energy levels). This is taken into account by the Fermi-Dirac distribution, which is a probability that the state of the ideal electron gas at constant temperature is occupied

$$f(E) = \frac{1}{e^{(E-\mu)/k_BT} + 1} \tag{82}$$

where μ is the chemical potential and depends on temperature and the number of particles. For non-zero thermodynamic temperatures it has a value of 1/2 while at absolute zero the chemical potential is equal to the so-called Fermi energy E_F, which is defined as *the energy of the highest occupied state at absolute zero* [21]. However, as the system is heated up, not all electrons are excited by the energy k_BT. Rather than that, only electrons in a range of k_BT around the Fermi level absorb the energy in orders of k_BT.

For $k_B << E_F$, the electronic contribution to the heat capacity C_e can be derived from the increase of the total energy of the electron system U due to being heated up from zero to temperature T as

$$U = \int_0^\infty E\mathscr{D}(E)f(E)\mathrm{d}E - \int_0^{E_F} E\mathscr{D}(E)\mathrm{d}E \tag{83}$$

where $f(E)$ is the Fermi-Dirac distribution from Eq. 82 and $\mathscr{D}(E)$ is the number of states per energy, or *density of states*. The number of particles then is

$$N = \int_0^\infty \mathscr{D}(E)f(E)\mathrm{d}E \tag{84}$$

and can be multiplied by the Fermi energy

$$E_FN = E_F\int_0^\infty \mathscr{D}(E)f(E)\mathrm{d}E \tag{85}$$

Then we can take the temperature derivatives of Eq. 83 and 85 to obtain equations

$$C_e = \frac{\partial U}{\partial T} = \int_0^\infty E\mathscr{D}(E)\frac{\partial f(E)}{\partial T}\mathrm{d}E \tag{86}$$

$$0 = E_F\frac{\partial N}{\partial T} = \int_0^\infty E_F\mathscr{D}(E)\frac{\partial f(E)}{\partial T}\mathrm{d}E \tag{87}$$

and subtract the second from the first one

$$C_e = \int_0^\infty (E - E_F)\mathscr{D}(E)\frac{\partial f(E)}{\partial T}\mathrm{d}E \tag{88}$$

For low temperatures where $k_BT/E_F < 0.01$, we can consider the density of states $\mathscr{D}(E)$ to be

constant, because the derivative $\partial f(E)/\partial T$ is large only for energies around E_F

$$C_e \approx \mathscr{D}(E) \int_0^\infty (E - E_F) \frac{\partial f(E)}{\partial T} \mathrm{d}E \tag{89}$$

As mentioned at the beginning, the chemical potential μ at zero temperature is equal to Fermi energy E_F, and therefore

$$\frac{\partial f(E)}{\partial T} = \frac{E - E_F}{k_B T^2} \frac{e^{(E-E_F)/k_B T}}{\left[e^{(E-E_F)/k_B T} + 1\right]^2} \tag{90}$$

and so the electron heat capacity becomes [21]

$$C_e = \frac{1}{3} \pi^2 \mathscr{D}(E_F) k_B^2 T \tag{91}$$

4 Methodology

The quantum mechanical calculations were performed utilizing Vienna Ab-Initio Simulation Package (VASP) [30] implementing the PAW formalism. Used GGA was the one parametrized by Perdew-Burke-Enzerhof (PBE) [17].

Cutoff energy for the plane wave basis functions was set to 600 eV, used Γ-centered k-points grid was $8 \times 8 \times 8$ or equivalent in the case of pure uranium. For lattice dynamics calculations the $2 \times 2 \times 2$ supercells containing 160 atoms with the same Γ-centered k-points grid were used. For this purpose, PHONOPY code [28] was utilized, which used the direct force-constant method. Used convergence criteria for the total energy was set to 10^{-8} eV and 10^{-6}eV/Å for residual Hellmann-Feynman forces. For the case of U_2C_3, the SOI with the Hubbard U correction [31] is applied.

Bulk moduli-temperature dependencies were obtained using a fit to Vinet's equation of the state [33]. Elastic constants c_{ij} were obtained using AELAS program [32], which allows to fit the energy-strain relation with 7 distortions by quadratic polynomial.

5 Results and Discussion

5.1 Structural and Magnetic Properties

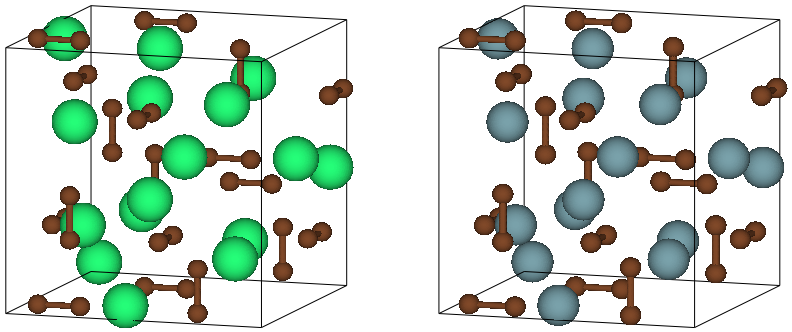

(a) Th_2C_3 (b) U_2C_3

Figure 1: Crystal structures of (a) Th_2C_3 and (b) U_2C_3. Big spheres and small spheres represent Th or U, and C atoms, respectively.

Experimental synthesis of Th_2C_3 via high pressure-high temperature methods showed the existence of a body-centered cubic structure, Pu_2C_3-type (space group $I\bar{4}3d$, No. 220), with the lattice parameter of 8.5555 Å [11, 34]. Calculated crystal structure is shown in Fig. 1. Similarly, the lattice parameter of U_2C_3 lies in the range from 8.0870 Å to 8.0899 Å [4, 35]. The comparison of calculated structural data for Th_2C_3 and U_2C_3 with experimental and other theoretical data is shown in Tab. 2.

	Method	Phase	a (Å)	C–C distance (Å)
Th_2C_3	PBE	NM	8.5599	1.4157
	exp. [11]	-	8.5555	-
U_2C_3	PBE	NM	8.0193	1.4654
	PBE	AFM	8.0477	1.3257
	PBE	FM	8.0399	1.4381
	PBE+SOI	FM	8.0585	1.4374
	PBE+SOI+U	FM	8.1061	1.4566
	exp. [4]	-	8.0870	-
	exp. [36]	-	8.0885	1.2950
	exp. [35]	-	8.0899	-
	theory [10]	NM	8.0970	1.4380

Table 2: Comparison of calculated structural data for Th_2C_3 and U_2C_3 with available literature.

For both phases, we investigated the magnetic ordering. Ferromagnetic (FM, along the direction [001]) and antiferromagnetic (AFM) ordering, inclusion of SOI and magnetism (ferromagnetic ordering only), and combination of SOI, ferromagnetism and Hubbard U model were utilized. Among the criteria to determine the phase stability is the comparison of the enthalpies of formation. In Fig. 2 the energy–volume relations are shown. The magnetic order doesn't play

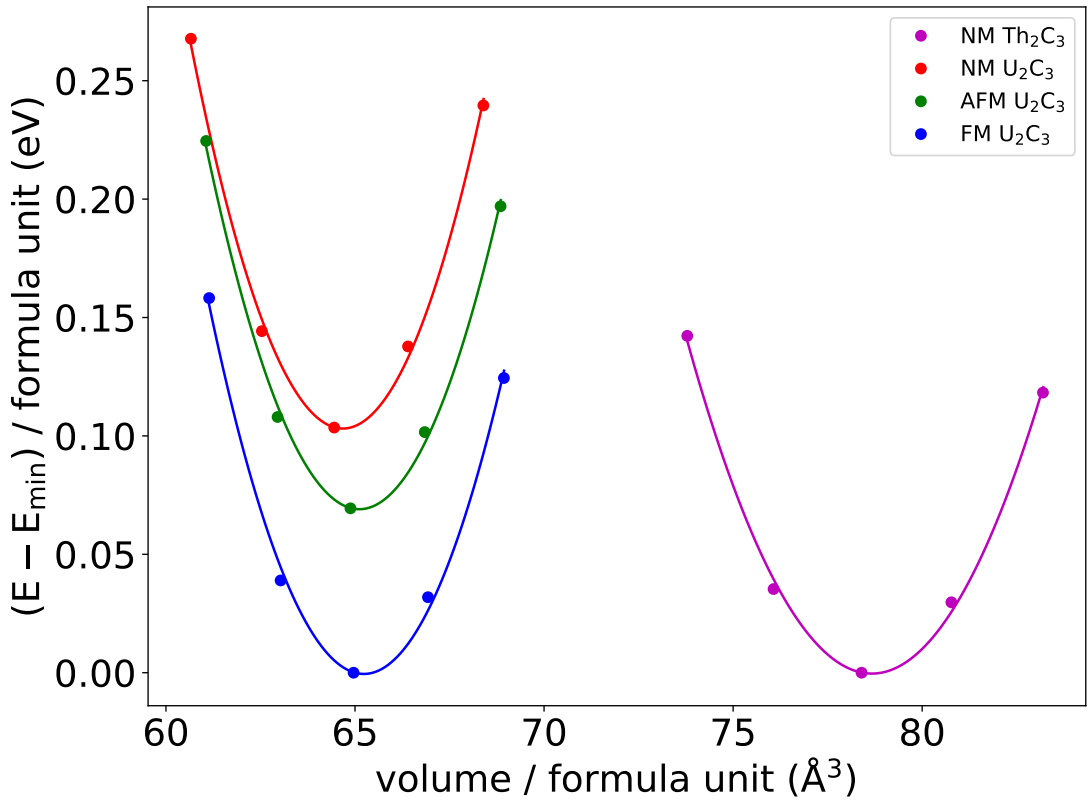

Figure 2: Total energy vs. volume dependencies of Th_2C_3 and U_2C_3. The ground state of the most stable magnetic ordering of the phase has been set to zero.

any role for Th_2C_3, which prefers the non-spin polarized solution. However, in the case of U_2C_3 the total energy for NM, FM and AFM magnetic orderings differs. The ground state possesses the ferromagnetic ordering, while the antiferromagnetic and non-magnetic are about 70 and 110 meV/formula unit higher in total energy, respectively. This certainly affects the enthalpy of formation, derived as

$$\Delta H_f = E_{\mathrm{Ac_2C_3}} - (2E_{\mathrm{Ac}} + 3E_{\mathrm{C}}) \tag{92}$$

where the Ac_2C_3 stands for a general actinide. The results shown in Tab. 3 indicate that the thorium sesquicarbide is more stable than the uranium one (has more *negative* enthalpy of formation).

	Method	Phase	ΔH_f (eV)
Th_2C_3	PBE	NM	−1.706
U_2C_3	PBE	NM	−1.037
	PBE	AFM	−1.060
	PBE	FM	−1.127
	PBE+SOI+U	FM	−1.428

Table 3: Enthalpy of formation of Th_2C_3 and U_2C_3. The values are per formula unit.

Shi et al. [10] employed a Hubbard U model to take into account the less itinerant behavior of uranium's $5f$ electrons, with U parameter around 3 eV. However, this model is clearly not sufficient, as seen from the comparison of calculated lattice parameters in Tab. 2. Here the results close to the to experimental values are achieved when one uses the model of a ferromagnetic ordering, while taking into account the SOI, and also employing the Hubbard model with $U = 0.5$ and $J = 0.5$ eV.

For ferromagnetic ordering of U_2C_3 with SOI and Hubbard U, the spin and orbital moments are 0.9 and -1.7 μ_B, respectively.

The occupied Wyckoff positions (internal parameters) of the most stable structures are 16c (0.0478, 0.0478, 0.0478) for Th and 24d (0.2923, 0, 0.25) for C, and 16c (0.0489, 0.0489, 0.0489) for U and 24d (0.2852, 0, 0.25) for C, for Th_2C_3 and U_2C_3, respectively.

5.2 Electronic Properties

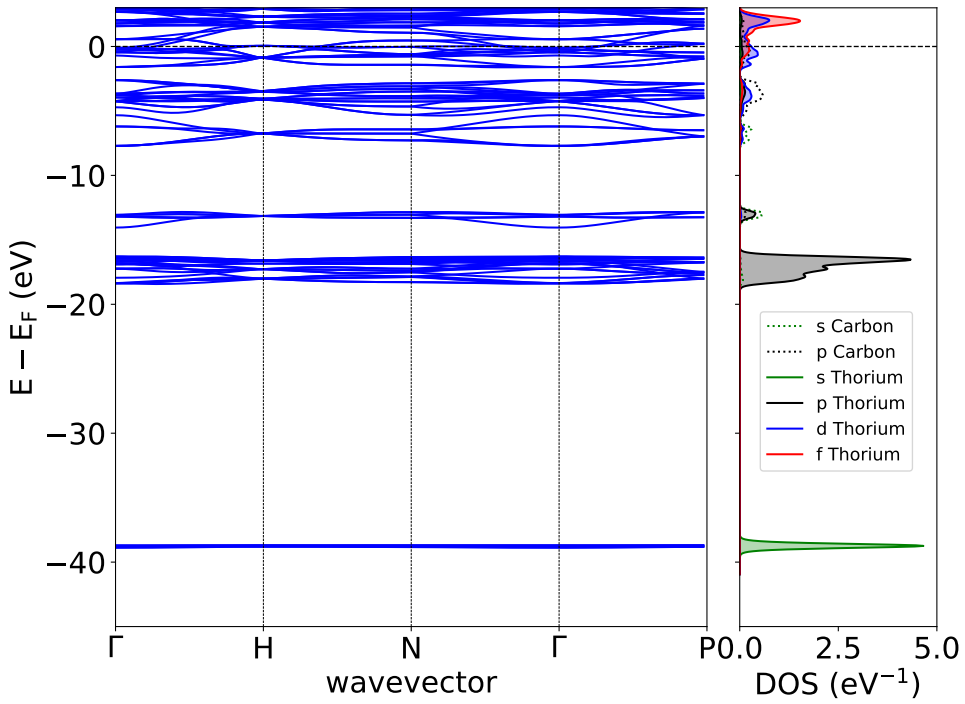

Figure 3: Band structure and density of states of Th_2C_3. The Fermi energy is set to zero, DOS is per atom.

We calculated the density of states (DOS) and the band structure (along high symmetry points) for non-spin polarized Th_2C_3 and ferromagnetic U_2C_3 with the inclusion of SOI and Hubbard U, see Fig. 3 and 4. Once the spin polarization is introduced, one can see the splitting of the valence bands (see Fig. 4). The non-magnetic U_2C_3 has 2.03 $5f$ electrons up to the Fermi level. This rises to 2.33 $5f$ electrons with the introduction of spin polarization. The inclusion of SOI and Hubbard U has a negligible effect on $5f$ occupancy, which rises to 2.35 $5f$ electrons. The ferromagnetism in U_2C_3 is therefore caused by the $5f$ electrons. This also explains why Th_2C_3 is non-magnetic, since it has too few $5f$ electrons, as one thorium atom in Th_2C_3 has

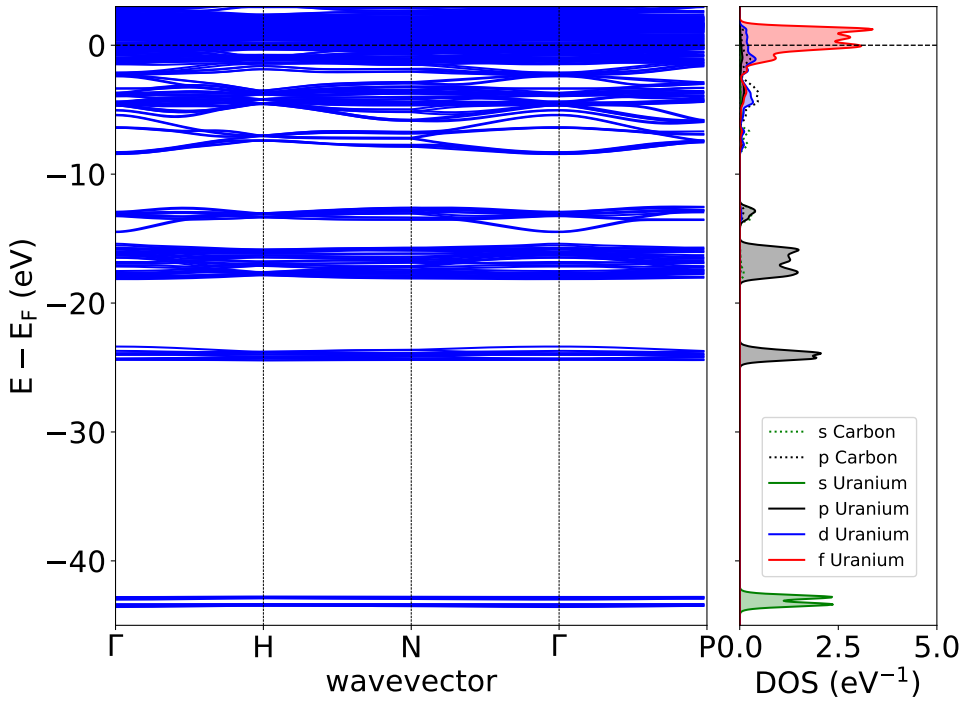

Figure 4: Band structure and density of states of U_2C_3 with SOI and Hubbard U. The Fermi energy is set to zero, DOS is per atom.

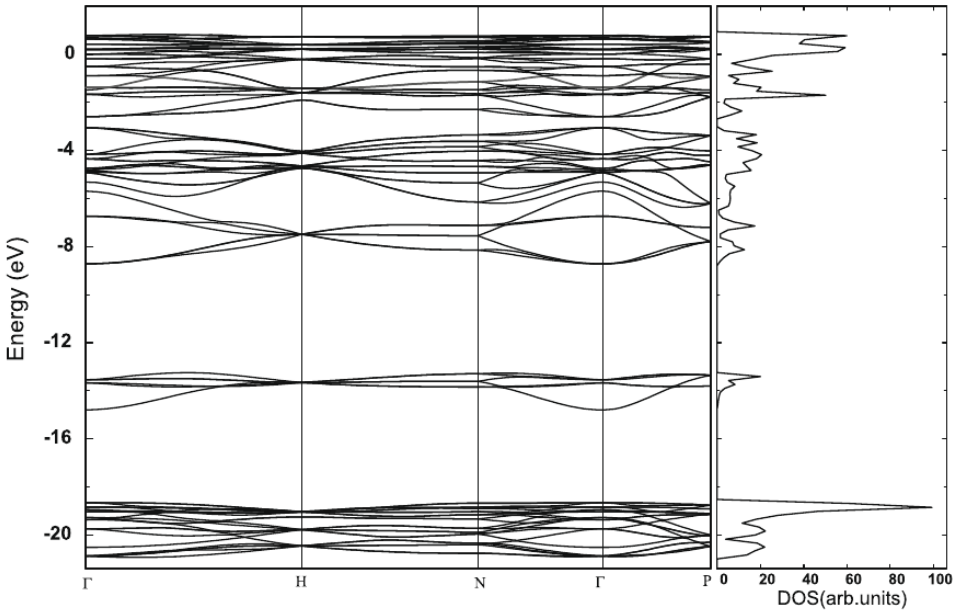

Figure 5: U_2C_3 band structure and density of states of Shi et al [10]. The Fermi energy is set to zero.

in its ground state 0.35 $5f$ electrons, compared to uranium in U_2C_3, which has $\approx 7\times$ more $5f$ electrons.

Core s electrons of U and Th lie around the energy of 40 eV below Fermi level, highly delocalized $6d$ electrons are spread 8 eV below Fermi energy and higher, $5f$ electrons have the

highest density close to the Fermi level. $5f$ electrons show their typical dual nature, as they cannot be said to be fully localized nor completely itinerant. The most noticeable effect of the band splitting can be seen in $6p$ electrons of uranium as a large amount of their density has been shifted closer to the Fermi energy due to the effect of SOI. The most prevalent states at the Fermi level are $5f$ for uranium sesquicarbide, while for thorium the $5f$ and $6d$ are equal. These are the states dominating their respective chemical bonding.

For carbon, s electrons are located at 7 and 14 eV below the Fermi level, while the p electrons are going from the Fermi energy to -7 eV, with the highest densities at 5 eV below the Fermi energy and close to it.

5.3 Elastic Properties

Experimental measurements of the elastic properties of Th_2C_3 and U_2C_3 are not known, while theoretical prediction has been made only for the case of U_2C_3 [10]. Comparison of our data with this study can be seen in Tab. 4.

The largest difference in calculated elastic properties can be seen for elastic constant c_{11}, which is around 20 %. The study of Shi et al. did not take into account any magnetic ordering, and therefore his prediction of elasticity concerns meta-stable state, and not the true ground state.

	Method	Phase	c_{11}	c_{12}	c_{44}	P_c	A_Z	E	G	B	G/B	ν
Th_2C_3	PBE	NM	310	96	84	12	0.79	234	92	167	0.55	0.27
U_2C_3	PBE	NM	373	149	112	37	1.00	289	112	223	0.50	0.29
	PBE	FM	379	127	115	12	0.91	301	119	211	0.57	0.26
	PBE+SOI+U	FM	311	129	101	27	1.11	249	97	189	0.51	0.28
	theory [10]	NM	383	121	91	30	0.69*	238*	91*	208	0.44*	0.31*

Table 4: Comparison of calculated elastic properties for Th_2C_3 and U_2C_3. All the relevant values are given in GPa. Values marked by a star were calculated from the $G = c_{44}$ identity for isotropic crystals and other relationships discussed in section 3.3.4.

The Cauchy pressure P_C is two times higher for U_2C_3, meaning its two times more isotropic than the Th_2C_3. The Pugh ratio G/B, a measure used for the comparison of ductility of similar structures, is 7 % lower for U_2C_3, showing that the Th_2C_3 is less ductile. The comparison of Zener anisotropy and c_{44} shows that the U_2C_3 is more resistive to the elongation along the body diagonal, while Th_2C_3 is more resistive to the deformation in z axis.

5.4 Thermodynamical Properties

Fig. 6 and 7 shows the calculated phonon spectra of actinide sesquicarbides. The first 5 THz vibration frequencies are occupied by thorium and uranium. Carbon in thorium sesquicarbide occupies the frequencies at 5–10, 15 and 30–35 THz. The 15 THz frequency has been splitted to the states occupying 12 and 15 THz.

The resulting heat capacity can be seen in Fig. 8. The lattice (phononic) heat capacities C_V with and without the electronic contribution to the heat capacity C_e are in Fig. 8. The difference between the heat capacity of Th_2C_3 and U_2C_3 is negligible. However, the inclusion

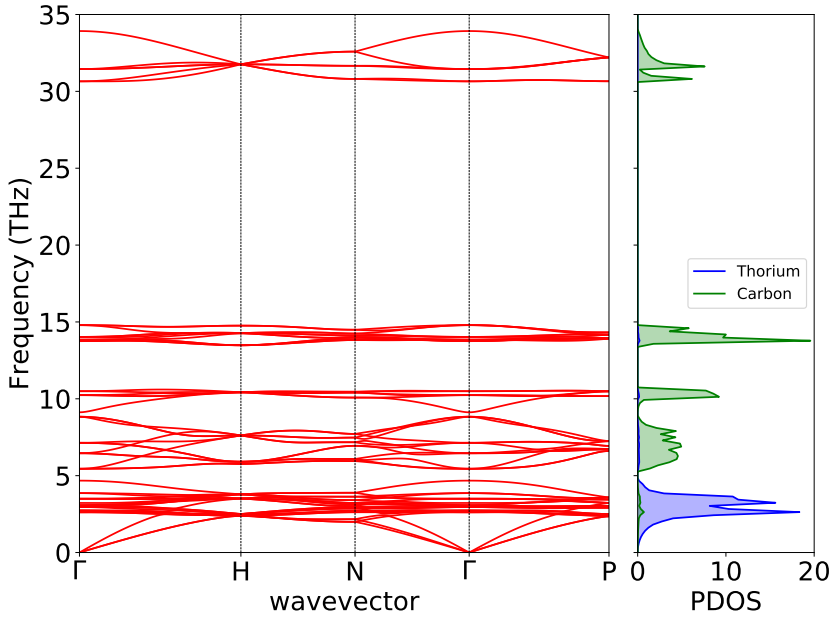

Figure 6: Phonon band structure and density of states of Th_2C_3.

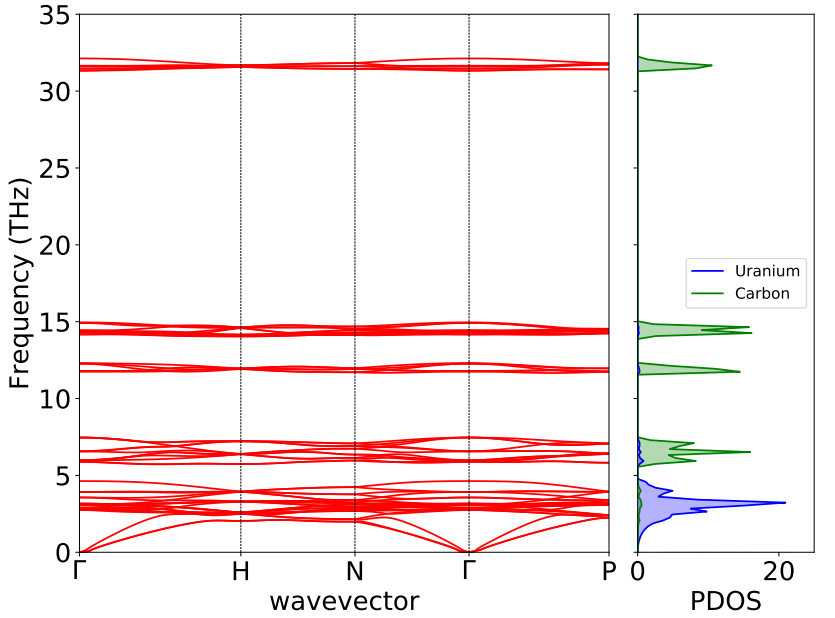

Figure 7: Phonon band structure and density of states of U_2C_3.

of the electronic contribution to the heat capacity C_e starts to show a difference at around 200 K and increases linearly with temperature. The difference between thorium and uranium sesquicarbide is about 2× for the uranium one due to the difference at the DOS at the Fermi level (which is two times larger for U_2C_3), upon which the electronic contribution directly depends.

The addition of the electronic heat capacity shows a very good correspondence to the experimental values of Andon et al. [37], from 0 to 320 K. A slight difference starts at around 250 K, as our calculations were made at constant volume, while the experiment at constant pressure.

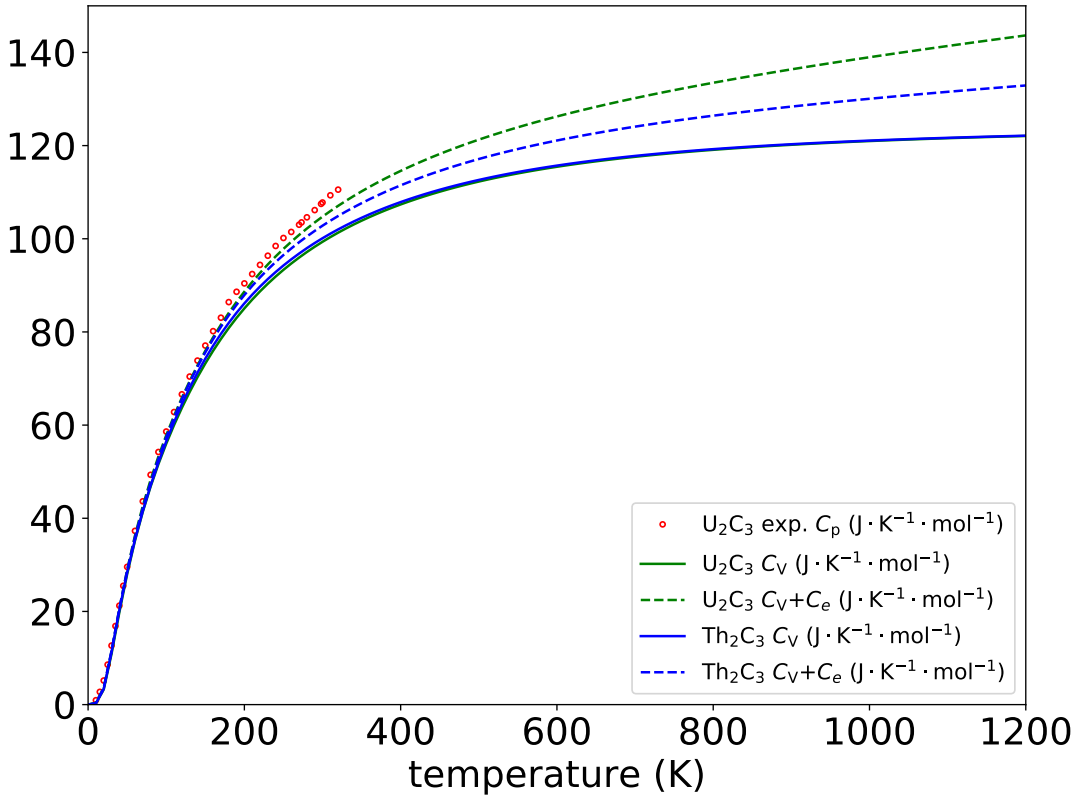

Figure 8: Calculated lattice and electronic heat capacity of Th_2C_3 and U_2C_3.

6 Conclusion

Electronic, structural, magnetic, mechanical and thermodynamic properties of Th_2C_3 and U_2C_3 were determined via first principles calculation. We found that for the accurate description of electronic structure of Th_2C_3 the SOI has a negligible effect. The U_2C_3 calculations included the SOI and Hubbard U model, since those were found to most accurately reflect the electronic structure and determined physical quantities with respect to the available experimental data.

The non-spin polarized calculation was not able to sufficiently reproduce the experimental values of the U_2C_3 lattice parameter, noticeably underestimating it. Inclusion of the SOI increased said lattice parameter, with a slight Hubbard U correction leading to its further increase.

From the determined enthalpy of formation it is found that the ferromagnetic ordering is the most stable one for U_2C_3. Magnetism was found to play no role in the phase stability of Th_2C_3. This is attributed to almost no presence of $5f$ electrons in thorium.

U_2C_3 was found to have significantly more $5f$ electrons. The electronic band structure is comparable to other theoretical study utilizing a non-spin polarized model with significantly higher Hubbard U correlation. The Fermi level of the uranium sesquicarbide is occupied predominantly by $5f$ states, while in the thorium one there is an equal presence of $6d$ and $5f$ states. Those are the states that participate in their respective chemical bonding.

Both non-spin polarized and spin polarized calculation of elastic constants agree with the calculation of Shi et al. The comparison to Th_2C_3 shows that overall elastic constants are lower than in U_2C_3, while the c_{11} is approximately the same for both compounds. According to the ratio of the shear and bulk moduli, the U_2C_3 is more ductile than Th_2C_3. The calculated Zener anisotropy also shows differences in materials response to deformation, with U_2C_3 being more resistive to the deformation along the body diagonal and Th_2C_3 along the z axis.

The calculated heat capacity at constant volume of U_2C_3 is in a good agreement with the experimental values. The difference in the heat capacity between the uranium and thorium sesquicarbide is caused by its electronic contribution dependent on the density of states at the Fermi level, which is two times higher in the case of U_2C_3.

This thesis has several important outcomes. U_2C_3 is a ferromagnetic compound, whose accurate description is dependent on the inclusion of SOI and small Hubbard U correlation. Calculations show that Th_2C_3 is non-magnetic and stable at 0 K and ambient pressure. The differences in their elastic and thermal properties are caused mainly by the higher number of $5f$ electrons in U_2C_3.

References

[1] MANES, L. *Actinides - chemistry and physical properties.* Berlin, Heidelberg: Springer-Verlag, 1985. ISBN 9783540390428.

[2] MORSS, L. R., N. M. EDELSTEIN, J. FUGER and J. J. KATZ. *The chemistry of the actinide and transactinide elements.* 3rd ed. Dordrecht: Springer, 2006. ISBN: 9781402035982.

[3] HOUSECROFT, Catherine E. and A. G. SHARPE. *Inorganic chemistry.* 4th ed. Harlow: Pearson, 2012. ISBN: 0273742752.

[4] WILSON, W. B. High-temperature X-ray diffraction investigation of the uranium-carbon system. Journal of the American Ceramic Society. 1960, 43(2), 77–80. DOI: 10.1111/j.1151-2916.1960.tb13644.x

[5] SEARS, M. B. and L. M. FERRIS. Studies on the U-C constitutional diagram between UC and UC_2. *Journal of Nuclear Materials*, 1969. **32**(1), 101-112. DOI: 10.1016/0022-3115(69)90145-7.

[6] HOLLEY Jr., Charles E. Thermodynamic properties of actinide carbides. *Journal of Nuclear Materials*, 1974. **51**(1), 36-46. DOI: 10.1016/0022-3115(74)90112-3.

[7] CARLSON, O. N. and E. R. STEVENS. Thorium phase diagrams. *Nuclear Engineering and Design*, 1971. **17**(3), 439-446. DOI: 10.1016/0029-5493(71)90104-X.

[8] WDOWIK, U. D., P. PIEKARZ, D. LEGUT and G. JAGŁO. Effect of spin-orbit and on-site Coulomb interactions on the electronic structure and lattice dynamics of uranium monocarbide. *Physical Review B.* 2016, **94**(5). DOI: 10.1103/PhysRevB.94.054303.

[9] KÝVALA, L. and D. LEGUT. Lattice dynamics and thermal properties of thorium metal and thorium monocarbide. *Physical Review B*, 2020. **101**(7). DOI: 10.1103/PhysRevB.101.075117.

[10] SHI, Hongliang, P. ZHANG, S.-S. LI, B. WANG and B. SUN. First-principles study of UC_2 and U_2C_3. *Journal of Nuclear Materials.* 2010, **396**, 218-222. DOI: 10.1016/j.jnucmat.2009.11.009.

[11] KRUPKA, M. C. High pressure synthesis of thorium sesquicarbide: a new actinide carbide. *Journal of the Less-Common Metals*, 1970. **20**(2), 135-140. DOI: 10.1016/0022-5088(70)90098-6.

[12] VVEDENSKY, D. D. Quantum Theory of Electrons in Solids, London: The Blackett Laboratory, Imperial College, 2000-2001.

[13] PATTERSON, James D. and Bernard C. BAILEY. *Solid-state physics: introduction to the theory.* Third edition. Springer International Publishing, 2018. ISBN: 9783319753225.

[14] BÖER, Karl W. and Udo W. POHL. *Semiconductor physics.* Switzerland: Springer International Publishing, 2018. ISBN: 9783319691503.

[15] HOHENBERG, P. and W. KOHN. Inhomogeneous electron gas. *Physical Review*. 1964, **136**(3B), 864-871. DOI: 10.1103/PhysRev.136.B864.

[16] KOHN, W. and L. J. SHAM. Self-consistent equations including exchange and correlation effects. *Physical Review*. 1965, **140**(4A), 1133-1138. DOI: 10.1103/PhysRev.140.A1133.

[17] PERDEW, J. P., K. BURKE and M. ERNZERHOF. Generalized Gradient Approximation Made Simple. *Physical Review Letters*. 1996, **77**(18), 3865-3868. DOI: 10.1103/PhysRevLett.77.3865. ISSN 00319007.

[18] SLATER, J. C. Wave functions in a periodic potential. *Physical Review*. 1937, **51**(10), 846-851. DOI: 10.1103/PhysRev.51.846. ISSN 0031899X.

[19] BLUNDELL, Stephen. *Magnetism in condensed matter*. Oxford University Press, 2001. ISBN: 0198505922.

[20] PAVARINI, Eva, Erik KOCH, Frithjof ANDERS and Mark JARRELL, ed. *Correlated electrons: from models to materials*. Germany: Forschungszentrum Jülich, 2012, **Modeling and Simulation, Vol. 2**. ISBN 978-3-89336-796-2.

[21] KITTEL, Charles. *Introduction to solid state physics*. New York: John Wiley & Sons, 1996. ISBN: 0-471-11181-3.

[22] ASHCROFT, Neil W. and N. David MERMIN. *Solid state physics*. Saunders College Publishing, 1976. ISBN: 0-03-083993-9.

[23] MARTIN, Richard M. *Electronic structure: basic theory and practical methods*. United Kingdom: Cambridge University Press, 2004. ISBN: 0521782856.

[24] GRIMVALL, Göran. *Thermophysical properties of materials*. Enl. and rev. ed. New York: Elsevier, 1999. ISBN 0444827943.

[25] PUGH, S. F. Relationships between the elastic moduli and the plastic properties of polycrystalline pure metals. *Philosophical Magazine*. 1954, **45**(367), 823-843. DOI: 10.1080/14786440808520496. ISSN: 19415990.

[26] KAXIRAS, Efthimios. *Atomic and electronic structure of solids*. New York: Cambridge University Press, 2003. ISBN: 9780521523394.

[27] SOUBUSTA, Jan. *Fyzika pevných látek SLO/PL*. Olomouc: Univerzita Palackého v Olomouci, 2012. ISBN 9788024430959.

[28] TOGO, A. and I. TANAKA. First principles phonon calculations in materials science. *Scripta Materialia*. 2015, **108**, 1-5. DOI: 10.1016/j.scriptamat.2015.07.021. ISSN 13596462.

[29] DOVE, Martin T. *Introduction to lattice dynamics*. Cambridge University Press, 1993. ISBN: 0-521-39293-4.

[30] KRESSE, G. and J. FURTHMÜLLER. Efficient iterative schemes for ab initio total-energy calculations using a plane-wave basis set. *Physical Review B*. 1996, **54**(16), 11169-11186. DOI: 10.1103/PhysRevB.54.11169. ISSN 01631829.

[31] DUDAREV, S. L., G. A. BOTTON, S. Y. SAVRASOV, C. J. HUMPHREYS and A. P. SUTTON. Electron-energy-loss spectra and the structural stability of nickel oxide: An LSDA+U study. *Physical Review B*. 1998, **57**(3), 1505-1509. DOI: 10.1103/PhysRevB.57.1505. ISSN 01631829.

[32] ZHANG, S. H. and R. F. ZHANG. AELAS: Automatic ELAStic property derivations via high-throughput first-principles computation. *Computer Physics Communications*. 2017, **220**, 403-416. DOI: 10.1016/j.cpc.2017.07.020.

[33] VINET, P., J. FERRANTE, J. H. ROSE and J. R. SMITH. Compressibility of solids. *Journal of Geophysical Research*. 1987, **92**(B9), 9319-9325. DOI: 10.1029/JB092iB09p09319. ISSN 01480227.

[34] YANG, R., B. TANG, T. GAO and B. Y. AO. Density functional study of Pu_2C_3. *The European Physical Journal B*. 2017, **90**(8). DOI: 10.1140/epjb/e2017-70749-8.

[35] HENNECKE, J. F. A. and C. J. TOUSSAINT. The lattice parameter and X-ray powder pattern of U_2C_3. *Journal of Applied Crystallography*. 1969, **2**(6), 301-303. DOI: 10.1107/s0021889869007254.

[36] AUSTIN, A. E. Carbon positions in uranium carbides. *Acta Crystallographica*. 1959, **12**(2), 159-161. DOI: 10.1107/s0365110x59000445.

[37] ANDON, R. J. L., J. F. COUNSELL, J. F. MARTIN and H. J. HEDGER. Thermodynamic properties of uranium compounds. Part 1.—Low-temperature heat capacity and entropy of three uranium carbides. *Transactions of the Faraday Society*. 1964, **60**(0), 1030–1037. DOI:10.1039/tf9646001030.

Acknowledgement

This bachelor thesis was supported by the European Regional Development Fund in the IT4Innovations national supercomputing center - Path to Exascale project, No. CZ.02.1.010.00.016_0130001791 within the Operational Programme Research Development and Education and by Czech Science Foundation project No. 17 − 27790S.